Water Research 155 (2019) 152–161

Contents lists available at ScienceDirect

Water Research

journal homepage: www.elsevier.com/locate/watres

Slippery for scaling resistance in membrane distillation: A novel porous micropillared superhydrophobic surface

Zechun Xiao [a, b], Rui Zheng [a, b], Yongjie Liu [a, c], Hailong He [c], Xiaofei Yuan [d], Yunhui Ji [e], Dongdong Li [a], Huabing Yin [d, **], Yuebiao Zhang [c], Xue-Mei Li [a], Tao He [a, d, *]

[a] Shanghai Advanced Research Institute, Chinese Academy of Sciences, Shanghai, 201210, China
[b] University of Chinese Academy of Sciences, Beijing, 100049, China
[c] School of Physical Science and Technology, ShanghaiTech University, Shanghai, 201210, China
[d] School of Engineering, University of Glasgow, Glasgow, G12 8LT, UK
[e] National Laboratory of Solid State Microstructures, Collaborative Innovation Center of Advanced Microstructures, College of Engineering and Applied Sciences, Department of Materials Science & Engineering, Nanjing University, Jiangsu, 210093, China

ARTICLE INFO

Article history:
Received 15 September 2018
Received in revised form
8 January 2019
Accepted 9 January 2019
Available online 1 February 2019

Keywords:
Micromolding phase separation
Surface pattern
Slippery
Membrane distillation
Scaling
Membrane

ABSTRACT

Scaling in membrane distillation (MD) is a key issue in desalination of concentrated saline water, where the interface property between the membrane and the feed become critical. In this paper, a slippery mechanism was explored as an innovative concept to understand the scaling behavior in membrane distillation for a soluble salt, NaCl. The investigation was based on a novel design of a superhydrophobic polyvinylidene fluoride (PVDF) membrane with micro-pillar arrays (MP-PVDF) using a micromolding phase separation (μPS) method. The membrane showed a contact angle of $166.0 \pm 2.3°$ and the sliding angle of $15.8 \pm 3.3°$. After CF_4 plasma treatment, the resultant membrane (CF_4-MP-PVDF) showed a reduced sliding angle of 3.0°. In direct contact membrane distillation (DCMD), the CF_4-MP-PVDF membrane illustrated excellent anti-scaling in concentrating saturated NaCl feed. Characterization of the used membranes showed that aggregation of NaCl crystals occurred on the control PVDF and MP-PVDF membranes, but not on the CF_4-MP-PVDF membrane. To understand this phenomenon, a "slippery" theory was introduced and correlated the sliding angle to the slippery surface of CF_4-MP-PVDF and its anti-scaling property. This work proposed a well-defined physical and theoretical platform for investigating scaling problems in membrane distillation and beyond.

1. Introduction

Highly saline wastewater streams from steel, chemical, petrochemical, and mining industries are of key concern for environmental and economical sustainability in developing countries (Latorre, 2005; Shannon et al., 2008; Bouchrit et al., 2015; Choi et al., 2018; Deshmukh et al., 2018). Therefore, concentrating high salinity liquids has become an important task in water treatment. One of the main objectives in recent years is to concentrate close-to-saturation brine until zero-liquid-discharge (Yun et al., 2006; Shin and Sohn, 2016; Junghyun et al., 2017). Contemporary technologies, e.g. high pressure reverse osmosis (RO), electrodialysis (ED), mechanical vapor re-compression (MVR) and multi-effect distillation (Li et al., 2016) have been used, but all have different limitations. For example, RO and ED are powered by electricity, and are normally expensive. MVR and ED not only require high energy but also suffer from corrosion. Membrane distillation (MD) has attracted wide attention for desalinating highly concentrated brine with concentrations up to crystallization (Ji et al., 2010a; Nghiem et al., 2011; Edwie and Chung, 2013; Chen et al. 2014, 2015, 2017a, 2017b; Hickenbottom and Cath, 2014; Naidu et al. 2014, 2018; Bouchrit et al. 2015, 2017; Tian et al., 2015b; Eykens et al., 2016; Gryta, 2016; Shin and Sohn, 2016; Duong et al., 2017; Junghyun et al., 2017; Choi et al., 2018; Julian et al., 2018; Kim et al., 2018).

MD uses low grade heat or sustainable energy (such as solar power) and is potentially an affordable desalination technology (Alkhudhiri et al., 2012; Tijing et al., 2015; Eykens et al., 2017).

* Corresponding author. Shanghai Advanced Research Institute, Chinese Academy of Sciences, Shanghai, 201210, China.
** Corresponding author.
E-mail address: het@sari.ac.cn (T. He).

https://doi.org/10.1016/j.watres.2019.01.036
0043-1354/© 2019 Elsevier Ltd. All rights reserved.

Normally, a MD system is compact, lightweight, and resistant to corrosion. However, similar to other membranes, MD membranes are prone to fouling, scaling and membrane wetting (Tijing et al., 2015), which will lead to deteriorated performance. For high salt solutions, in particular when the concentration of salt approaches saturation, scaling becomes the most serious problem (Ji et al., 2010a; Gryta, 2011; Edwie and Chung, 2013; Chen et al., 2014; Hickenbottom and Cath, 2014; Nariyoshi et al., 2016; Bouchrit et al., 2017; Jiang et al., 2017; Tang et al., 2017; Julian et al., 2018; Zou et al., 2018). Crystals attached to the membrane surface alter surface wettability (e.g. from hydrophobic to hydrophilic), allowing continuous crystal growth into membrane pores and consequently membrane wetting (Yun et al., 2006; Gryta, 2008; Ramezanianpour and Sivakumar 2014). Wetted membranes result in free diffusion of salt molecules from the high salinity feed to the permeate, thus reducing membrane rejection. Although the consequence of scaling can be measured, the mechanism governing scaling is unknown. How to prevent scaling remains a significant challenge in membrane technology.

Observations of NaCl scaling have been reported in the literature. When treating 18 wt% NaCl brine in direct contact membrane distillation (DCMD), a critical size of 25 μm was found for the crystals on the PVDF membrane surface, which acted as initial growth sites and led to the full membrane coverage (Chen et al., 2014). Single NaCl crystals of 40 μm were also reported in a membrane distillation-crystallization (MDC) process, where about 9–16% of the total crystals were on the membrane surface and the piping (Nariyoshi et al., 2016). Scaling often occurred when the feed reached saturation (Bouchrit et al. 2015, 2017; Gryta, 2016). Injection of air (Choi et al., 2017) and increase of the feed flow velocity (Naidu et al., 2014; Choi et al., 2017) can mitigate scaling. However, when optimization of process parameters such as flow rate and temperature reversal were used to mitigate rapid flux decline in concentrating salt lake brine, there was little successes (Hickenbottom and Cath, 2014).

Instead of optimizing process parameters, membrane modification provides another important route to mitigate or prevent scaling. An electrically conducting membrane surface can be made by coating a carbon nanotube/poly(vinyl alcohol) (PVC) layer onto a polypropylene support, which can effectively dissolve silicate scale during desalination of geothermal brine (Tang et al., 2017). It has been shown that air bubbles can be created on the superhydrophobic surface of a perfluorodecyl acrylate modified poly(vinyldene fluoride) PVDF membrane (i.e. via initiated chemical vapor deposition, iCVD), which can suppress MD fouling despite increased crystal formation (Warsinger et al., 2016). However, in another study, a superhydrophobic membrane prepared by coating TiO_2 nanoparticles on a PVDF electrospun nanofiber support followed by chemical fluorosilanization, promoted more uniform and slower crystal formation and removal of the crystal deposition was easy (Razmjou et al., 2012; Meng et al. 2014b, 2015).

The majority of research on superhydrophobic membranes are based on chemical modification and/or the design of hierarchical structure (Razmjou et al., 2012; Wei et al., 2012; Meng et al. 2014a, 2014b, 2015; Yang et al. 2014, 2015; Tian et al., 2015b; Lee et al., 2016a; Tijing et al., 2016; Warsinger et al., 2016; Ren et al., 2017). Contradictory results were often observed (e.g. the examples above). These might be due to variations in the feed as well as undefined surface morphology. An intuitive assumption in MD is the existence of a static membrane/liquid interface. Therefore, it has been believed that mimicking the hierarchical structure of lotus leaves could provide an anti-fouling solution. However, actual fouling/scaling in MD occurs at triple-phase interfaces consisting of liquid phase (feed) – air phase (in pores) – solid phase (polymer). If the tri-phase interfaces are not always static, scaling can occur in different ways. The mechanisms underlying fouling and scaling in MD is highly complex. To address this challenge, our vision is to design a simple, but structurally well-controlled membrane surface that can modulate the interface properties and provide a dynamic contact line between the membrane and water phase.

Advances in nanofabrication technology have been used to create superhydrophobic surfaces (Li et al., 2007, 2008b; Xue Mei Li, 2007) and surfaces with multidimensional roughness (Kim et al., 2016). A recent study shows that MD membranes patterned with a groove structure have a weak hydrophobic interaction with BSA proteins and hence low fouling propensity (Xie et al., 2017). However, since the evaluation was in static conditions, information on scaling was not available. Similarly, corrugated PVDF membranes demonstrate the ability to alleviate salt deposition and fouling in DCMD of real seawater (Kharraz et al., 2015), but the dynamics of scaling was unknown.

Here, we attempt to understand the dynamic mechanisms of scaling at the liquid-air-solid interface in MD. For the first time, a patterned superhydrophobic PVDF membrane with porous micropillars was prepared via a micro-molding phase separation (μPS) technique. A similar technique has been used to create macropatterned surfaces for pressure driven membranes (Çulfaz et al. 2010, 2011a, 2011b; Hashino et al., 2011; Won et al. 2012, 2016; Jamshidi Gohari et al., 2013; Lee et al., 2013; Gençal et al., 2015; Maruf et al., 2016; ElSherbiny et al., 2017). However, pressure driven processes only involve a liquid-solid interface with a convective flow of liquid across the membrane. Therefore, it is fundamentally different from the vapor diffusion-based MD process. Here, porous micro-pillar formation together with CF_4 plasma treatment allowed the creation of a superhydrophobic PVDF membrane, which is employed to investigate: (1) the relationship between the micro-pattern and the hydrophobicity of the membrane surface; and (2) the relationship between the micro-pattern and the scaling property in DCMD for highly concentrated NaCl solutions. The superhydrophobic membrane demonstrated excellent anti-scaling properties when used to treat a saturated NaCl solution by DCMD. The results lend us to propose a “slippery surface” as a dynamic means of preventing scaling in MD. The novel multiscale hierarchical surface illustrated in this work also offers a promising platform for understanding and mitigating the scaling and fouling problems in other processes beyond MD.

2. Materials and methods

2.1. Materials and chemicals

PVDF (Solef 1015) was kindly supplied by Solvay. *N,N*-Dimethylacetamide (DMAc, AR) and Diethylene glycol (DEG, AR) were purchased from Sinopharm Chemical Reagent Co. Ltd and used without further purification. The silicon wafer mold with a pillar array was designed in house. The dimensions of the pillars are 5 μm in diameter (D), 10 μm in height (H) and 10 μm in period (P) (Fig. 1). A commercial flat sheet polyvinylidene fluoride membrane (abbreviated as C-PVDF, GVHP, Millipore, USA) with a nominal pore size of 0.22 μm and thickness of 125 μm was used as a benchmark.

2.2. Fabrication of polydimethylsiloxane (PDMS) mold

Oligomer PDMS and the curing agent (SYLGARD 184, Dow Corning Co. Ltd) were pre-mixed at a weight ratio of 10:1. After degassing in vacuum for 10 min, the mixture was cast onto the silicon wafer template. Then the wafer and the PDMS solution was transferred into a vacuum oven and cured for 3 h at 60 °C. The PDMS replica was then peeled off and stored in a clean container. The entire process was carried out in a clean room.

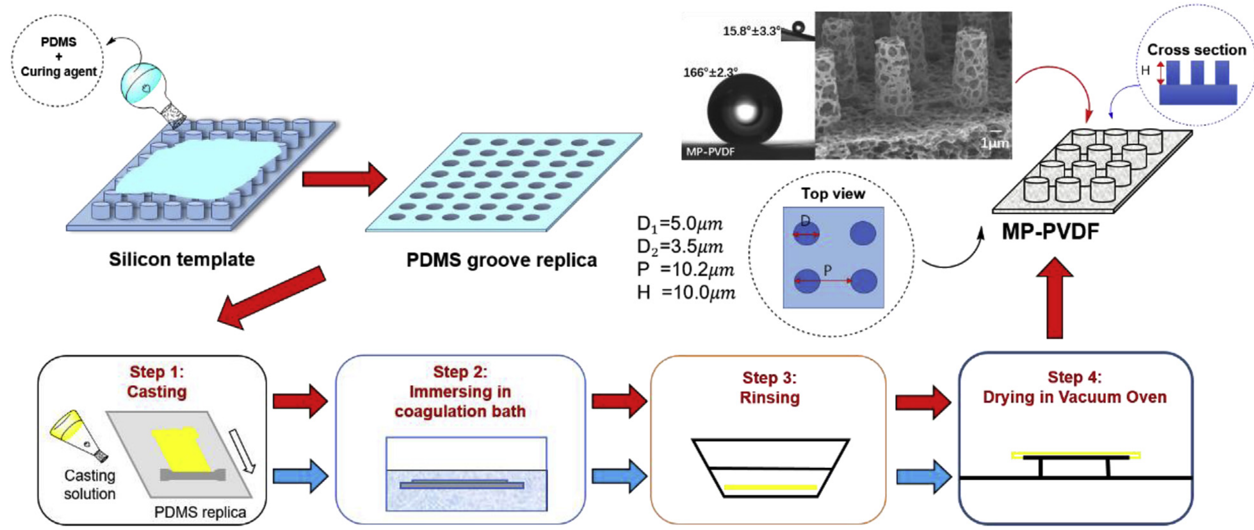

Fig. 1. Schematic for the fabrication of micro-pillar PVDF membranes (MP-PVDF). The silicon wafer mold has pillars with the dimension of 5 μm (diameter), 10 μm (height) and 10 μm (period). (For interpretation of the references to colour in this figure legend, the reader is referred to the Web version of this article.)

2.3. Fabrication of MP-PVDF membrane

A PVDF casting solution (PVDF/DEG/DMAc, 15/27.4/57.6 wt%) was prepared by mixing the components in a flask at 90 °C and agitated for 12 h. The polymer solution was then filtered using a metal filter of 40 μm. The casting solution was kept at 90 °C to degas. Fig. 1 shows the procedure for the fabrication of micro-pillar PVDF membranes and details are as follows.

An appropriate amount of the PVDF solution was spread uniformly on the PDMS replica on top of a glass plate to a thickness of 600 μm using a home-made stainless-steel casting knife. The solution was exposed to water vapor for 10 s (10 cm above a coagulation water bath, 75 °C) and then immersed in the coagulation bath for 15 min to induce precipitation. Upon precipitation, the membrane delaminated from the replica spontaneously. After rinsing with water to remove solvent and additives, ethanol was used to rinse the membrane before being dried in a vacuum oven at ambient temperature for 48 h. The resultant membrane is denoted as micro-pillared PVDF membrane (MP-PVDF).

2.4. Membrane modification by CF4 plasma treatment

MP-PVDF membrane was further treated with CF_4 plasma (an IoN40 plasma system, PVA Tepla Co. Ltd) to improve its hydrophobicity based on our previous methods (Wei et al., 2012; Yang et al. 2014, 2015; Chen et al. 2017a, 2017b). In brief, the substrate was cleaned first under argon plasma at 45 W for 15s and then in CF_4 gas at a flow rate of 120 cm^3/min (SCCM) at 200 W for 15 min. After the CF_4 modification, the chamber was cleaned using an O_2 plasma at 200 W for 15 min to avoid any CF_4 deposition on the electrodes.

2.5. Membrane characterization

Water contact angle (CA) and sliding angle (SA) of the samples were measured using a contact angle goniometer (Maist Drop Meter A-100P) via the sessile drop method. The tilt angle at which the droplet started rolling off the surface was denoted as the sliding angle. Pore size and pore size distribution were analyzed using porometry (Porolux 1000, Supplementary information Method S1) (Wei et al., 2012; Yang et al. 2014, 2015; Chen et al. 2017a, 2017b). Scanning electron microscopy (HITACH TM-1000 and FEI Nova Nano SEM 450) was used to characterize membrane morphology. The sample was sputtered with a thin layer of gold in a vacuum prior to SEM characterization.

2.6. MD performance

A bench scale DCMD unit (Supplementary Data Fig. S1) developed previously (Wei et al., 2012; Yang et al. 2014, 2015; Chen et al. 2017a, 2017b) was used to evaluate scaling on the membranes using 4 wt% or 25 wt% NaCl solutions. For the MP-PVDF and CF_4-MP-PVDF membranes, the side with pillars was in contact with the feed. The conductivity of the permeate was regularly measured to identify the point when salts from the feed penetrate to the permeate. Since 25 wt% is close to the saturated concentration for a NaCl solution, the experimental duration was significantly reduced. The feed and the permeate temperatures were maintained at 60 ± 0.3 °C and 20 ± 0.3 °C respectively. The flux (J, kg/m^2·h) was calculated based on equation (1):

$$J = \Delta m / A \Delta t. \quad (1)$$

Where Δm (kg) is the amount of water transported from the feed to the permeate, Δt the interval of the collection (h) and A the membrane area (m^2).

3. Results and discussion

3.1. Morphology of the MP-PVDF membrane

Fig. 2 shows the SEM images of the top, bottom and cross-section of the commercial PVDF (C-PVDF) and micro-pillar PVDF (MP-PVDF) membrane. Both membranes show a porous top and bottom surface, as well as a macroporous cross-section. The surface porosity and pore size of MP-PVDF membranes appears to be lower than C-PVDF membranes. In addition, MP-PVDF membranes contain porous pillar arrays with open structure throughout (Fig. 2, inserts). For the sake of clarity, the membrane surface facing the feed is denoted as the top surface. In this study, the top surface of the MP-PVDF membrane (Fig. 2) was the one in contact with the PDMS replica. During membrane formation, phase separation

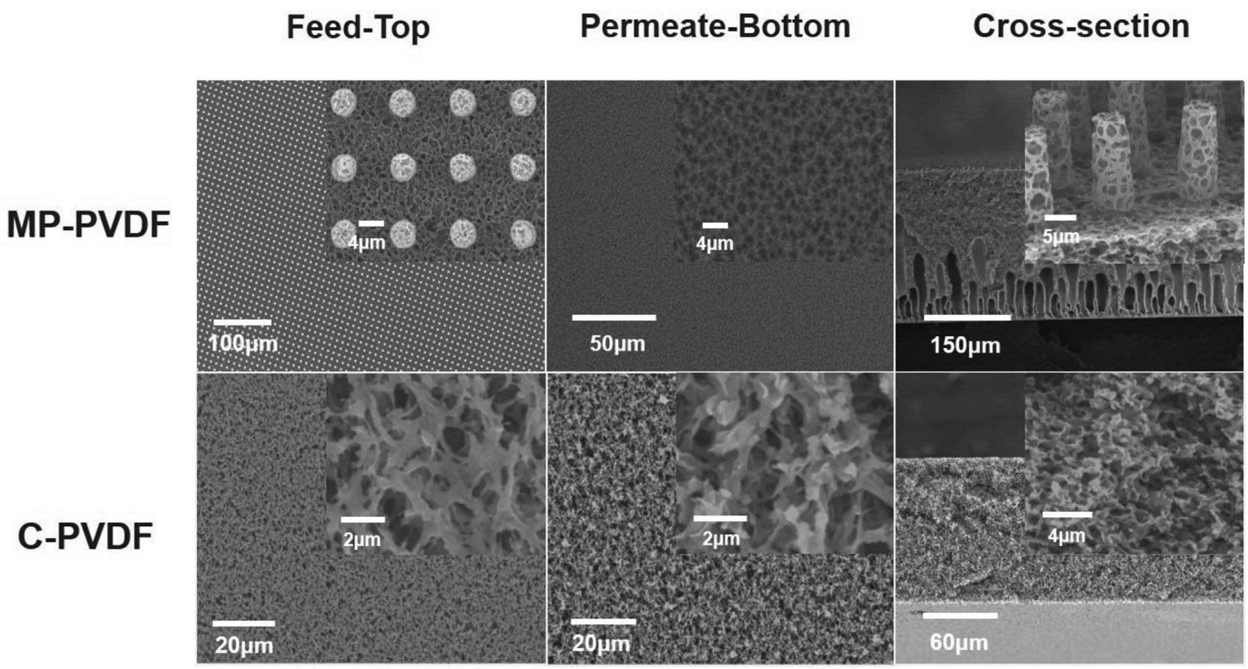

Fig. 2. SEM images of MP-PVDF and C-PVDF membranes. Feed-Top, Permeate-bottom and cross section. The top surface of MP-PVDF was slight tilted for a better view. Inserts are enlarged views.

started from the open surface of the polymer solution; instantaneous demixing occurred at the water/polymer solution interface, resulting in a finger-like macrovoid structure (i.e. MP-PVDF cross-section in Fig. 2). However, solvent and additives from the polymer solution within the PDMS replica had to diffuse through the whole membrane to the water bath and therefore it was a slow process. This allowed the polymer-lean phases to grow and eventually enlarge into micropores (He et al., 2003; Li et al. 2008b, 2010; Ji et al., 2010b). The interconnected porous structure in the top surface of the PVDF membrane is due to the competition between the solid-liquid phase separation and liquid-liquid separation for a semi-crystalline polymer (Xing et al., 2016). The open porous surface in the pillars is of particular interest for creating a super-hydrophobic surface.

The MP-PVDF membrane features an array of conical pillars of 5 μm at the bottom (i.e. the part connected to the bulk membrane) and 3.5 μm at the tip. Compared to the original pillar structure on the silicon mold, this reduction at the tip is likely caused by membrane shrinkage during phase separation. Nevertheless, the height and period for pillars on the membrane are the same as the designed silicon mold, i.e. 10 μm in both height and period.

As listed in Table 1, the MP-PVDF membrane has a thickness of ~264 μm, whereas the commercial PVDF membrane (C-PVDF) is of 130 μm. Attempts to reduce this thickness could be possible by controlling the casting process. Slightly higher porosity is found in MP-PVDF membranes (~79%) than C-PVDF membrane (75%), indicating a more open porous substrate in MP-PVDF. However, the mean pore size of MP-PVDF membranes (0.120 μm) is smaller than C-PVDF membranes (0.230 μm). Interestingly, the contact angle for MP-PVDF membranes (166.0 ± 2.3°) is significantly higher than that of C-PVDF membranes (139.2 ± 3.7°). The CF_4 plasma treatment may fluorinate membrane surfaces by F atom insertion or deposition of Teflon polymers (Yang et al. 2014, 2015; Tian et al., 2015b). This leads to a slightly enlarged mean pore size (i.e. from 0.120 μm to 0.201 μm), and further increased contact angle (i.e. from 166° to 176°). As shown in Fig. S2 (Supplementary Data), C-PVDF membrane possessed a narrow distribution of pore size, whereas C-PVDF and CF_4-MP-PVDF showed a relatively large pore size distribution.

The most striking difference is the sliding angle: C-PVDF membranes showed no sliding angle below 90°; MP-PVDF membranes showed a sliding angle of 15.8°; and CF_4-MP-PVDF showed a sliding angle of only 3.0°. The surface of CF_4-MP-PVDF membrane was so water repellent that a water droplet stuck to the needle rather than the membrane surface during the contact angle test. When the water droplet was released from the needle by a gentle flick, it rolled off the surface upon slight tilting. The surface energy follows a reverse order compared to the contact angle: C-PVDF membrane show the highest surface energy of 72 mJ/m^2, and CF_4-MP-PVDF membranes show the lowest energy of 0.27 mJ/cm^2. This

Table 1
Characteristics of the C-PVDF, MP-PVDF and CF_4-MP-PVDF membranes.

Membrane	C-PVDF	MP-PVDF	CF_4-MP-PVDF
Thickness/μm	132 ± 3	263 ± 2	264 ± 2
Mean pore size/μm	0.230 ± 0.0020.235 ± 0.013	0.078 ± 0.0120.120 ± 0.005	0.073 ± 0.0090.201 ± 0.013
Porosity (%)	75.3 ± 2.1	79.6 ± 3.7	78.9 ± 5.3
Contact angle/°	139.2 ± 3.7	166.0 ± 2.3	175.6 ± 1.3
Sliding angle/°	>90	15.8 ± 3.3	3.0 ± 0.8
Surface energy (mJ/m^2)[a]	71.8 ± 2.4	47.3 ± 0.6	0.27 ± 0.12

[a] Supplementary information Method S2 for determination of surface energy.

water repelling property and low surface energy of the CF_4-MP-PVDF membrane surface are not trivial characteristics, which are most probably related to the scaling/fouling process as shown in the experiments below.

Both MP-PVDF and CF_4-MP-PVDF membranes can be categorized as superhydrophobic due to their high contact angle and low sliding angles. The commercial PVDF membrane has a very open porous surface, but its contact angle was only 139°, and its sliding angle is above 90°. Water droplets on a hydrophobic surface are normally considered as either in the Cassie-Baxter state or in the Wenzel state (Li et al. 2007, 2008a; Xue Mei Li, 2007; Tian et al., 2015a). The difference between the two states is the contact areas between the water and the solid substrate: The Wenzel state is characterized by a larger contact area and more interaction between the liquid phase and solid phase, whereas air pockets between the liquid and solid phase are expected for the Cassie-Baxter state. Sliding angle is an indirect macroscopic feature indicating interaction between a surface and a water droplet. A sliding angle above 90°, is an indication of strong interaction between the surface and water. This minor, but very important information shows that the surface characteristics of the C-PVDF membrane is different from that of micropillared membrane (MP-VPDF and CF_4-MP-PVDF). For C-PVDF membranes, the water contact angle was found to be much higher than 90°, and no obvious wetting upon immersion in water was observed. However, if comparing to MP-PVDF and CF_4-MP-PVDF membranes with a high contact angle and low sliding angle, it is likely that water on C-PVDF surface is in a *meta*-Cassie-Baxter state with partial wetting. The cause might be related to the surface morphology: C-PVDF membrane has a homogeneous porous surface, but both MP-PVDF and CF_4-MP-PVDF have pillars with higher surface porosity. The state of water in contact with the membrane surface is not clear yet at this stage, but worthy of future analysis. Previous work on MD membranes with a superhydrophobic or omniphobic surface only considered static water contact angles, and did not measure sliding angles (Wei et al., 2012; Lin et al., 2014; Yang et al. 2014, 2015; Nejati et al., 2015; Tian et al., 2015b; Boo et al., 2016a, 2016b; Lee et al. 2016a, 2016b, 2016c; Tijing et al., 2016; Wang et al. 2016a, 2016b; Chen et al. 2017a, 2017b). In the MD process, water flows along the membrane surface, and thus behaves dynamically. Increasing the feed flow rate was reported to mitigate scaling (Naidu et al., 2014; Choi et al., 2017), which might be relevant to the dynamic behavior at the interface between water and membrane.

3.2. MD performance

Fig. 3 shows the flux and permeate conductivity using C-PVDF, MP-PVDF and CF_4-MP-PVDF membranes. An initial feed solution of 25 wt% NaCl was concentrated until changes in the flux or permeate conductivity occurred. We intentionally selected this close-to-saturation concentration to reduce the experiment time. With increased concentration, the C-PVDF membrane showed a gradual decrease in flux. When the concentration factor (i.e. the ratio of the salt concentration during the process to its initial concentration in the feed) reached about 1.1, the flux suddenly dropped to zero. A similar trend was found for the MP-PVDF membrane, but at a concentration factor of about 1.2. In contrast, CF_4-MP-PVDF membranes maintained a surprisingly stable flux at much higher concentration factors (i.e. 1.76). Initial tests using a 4 wt% NaCl feed solution showed no obvious variations in both flux and permeate conductivity for the three membranes. They were intact and remained integral (Supplementary information, Fig. S3). Reproducibility of the DCMD results was confirmed as shown in Supplementary Data, Fig. S4.

In terms of flux, CF_4-MP-PVDF showed a slightly higher initial flux than MP-PVDF. This is probably due to the enlarged effective evaporation surface area at the liquid-air-solid interface which contributed to the increased water flux (Yang et al. 2014, 2015). This difference gradually disappeared when the concentration factor reached 1.1, and after that both CF_4-MP-PVDF and MP-PVDF membranes showed a similar flux.

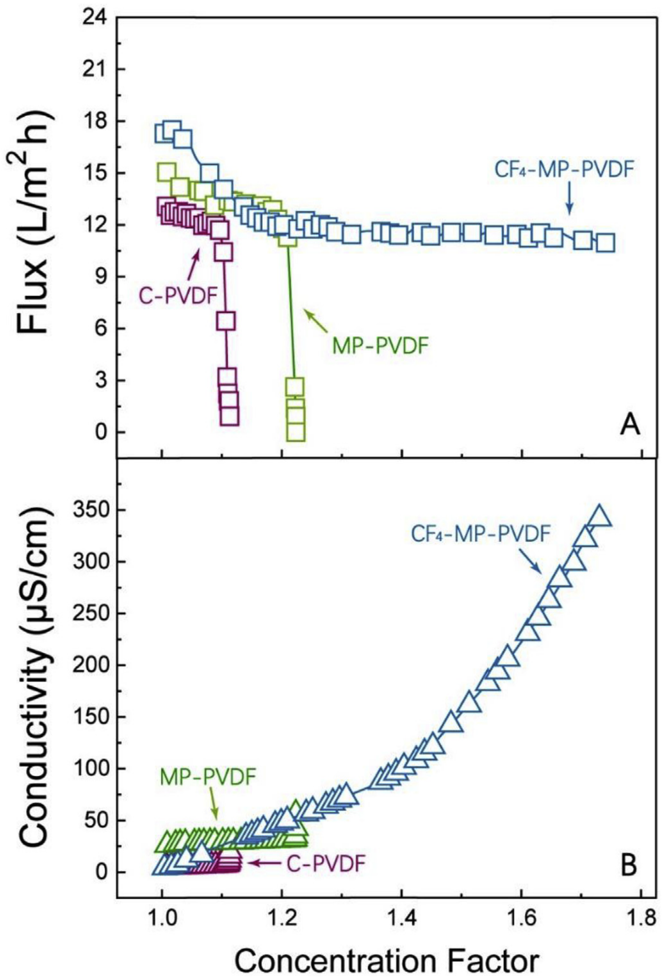

Fig. 3. DCMD performances of C-PVDF, MP-PVDF and CF_4-MP-PVDF membranes with an initial 25 wt % NaCl feed solution. A and B: Water flux and permeate conductivity of three membranes as a function of concentration factor. The feed temperature was maintained at 60 °C and the permeate temperature at 20 °C. The concentration factor is defined as the ratio of the salt concentration in the feed during the process to the initial salt concentration (i.e. 25 wt% NaCl).

In the case of permeate conductivity, very different results were obtained (Fig. 3B). The permeate conductivity of C-PVDF membranes increased gradually until a concentration factor of 1.1 (i.e. the flux declined to zero). Similar trend was observed for MP-PVDF membranes. For CF_4-MP-PVDF, the permeate conductivity increased continuously throughout the whole process until 350 μS/cm, without obvious sacrificing in MD flux. This phenomenon is striking in that saturated NaCl feed would generally cause instantaneously scaling and dramatic flux decline in MD (Tun et al., 2005; Gryta, 2010; He et al., 2013). Increase in permeate conductivity is an indication of diffusion of NaCl from saturated feed to the permeate; however, at the concentration factor of 1.76, the CF_4-MP-PVDF membrane showed a rejection of 99.9% (Supplementary Data Fig. S5). Although this value is very high, rigorous analysis would claim that current membrane is not perfect or other unknown mechanism exists. Minor defects in the membrane allow diffusion of

NaCl from feed to permeate; at low feed NaCl concentration, the diffusion of NaCl is minor thus the permeate conductivity does not show appreciable increase; but at saturation, diffusion of NaCl was noticed in the permeate. Besides the contribution of defects, the other contribution might be that the NaCl aerosols, generated at the interface from the saturated feed, eventually pass the porous hydrophobic pores and end in the permeate. Sea salt aerosols (SSA) have been routinely found at the marine boundary(Tyree et al., 2007; Jentzsch et al., 2011). We have to admit that this hypothesis is of no direct proof yet and requires further scientific investigation.

After the DCMD experiment, membrane samples were removed from the test cell and characterized as shown in Fig. 4. The contact angle for both C-PVDF and MP-PVDF membranes, was significantly reduced. The sliding angle of MP-PVDF membranes increased dramatically from 15.8° to above 90°, indicating that the surfaces became sticky to water. In contrast, the contact angle of CF_4-MP-PVDF membranes remained unchanged, but the sliding angle slightly increased from 3.3° to 10.5°. Optical images showed that the surfaces of CF_4-MP-PVDF on both feed and permeate sides remained clean. However, the surfaces of both C-PVDF and MP-

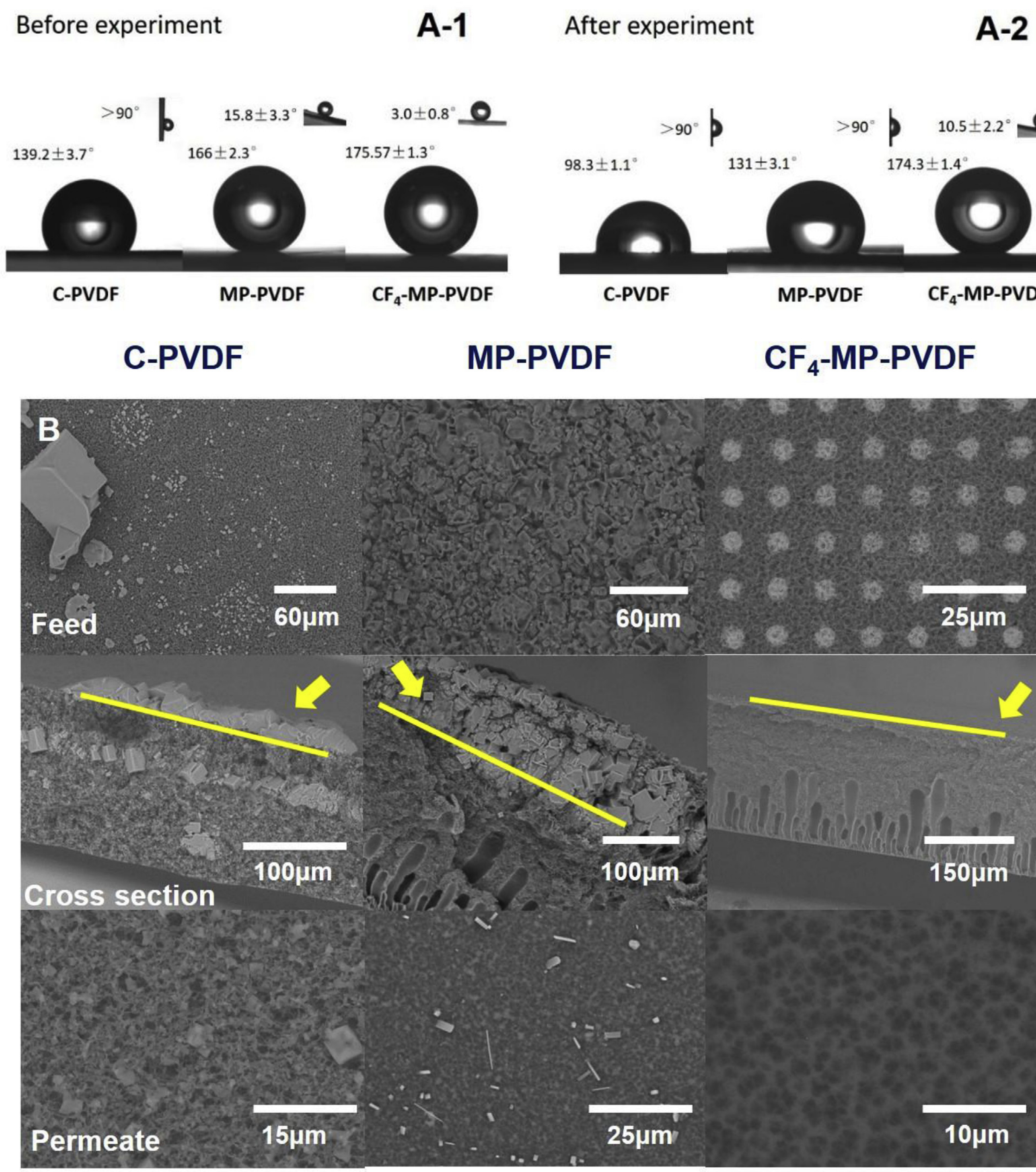

Fig. 4. Characteristics of C-PVDF, MP-PVDF and CF_4-MP-PVDF membranes before and after DCMD test. (A-1) and (A-2): contact angles and sliding angles of three membranes before and after DCMD; (B): SEM images of the surfaces and cross-section. For the cross-section images, arrows and lines indicate the membrane surface at the feed side. C-PVDF and MP-PVDF membranes showed aggregates of crystals.

PVDF membranes showed NaCl crystals (as highlighted by the red circles in Supplementary Data Fig. S6). This observation was further confirmed by the SEM images (Fig. 4B): a layer of NaCl crystals of various sizes were observed on the C-PVDF surface and some cubic crystals even imbedded in the middle of the support; furthermore, even permeate surface showed some cubic particulates which would be NaCl crystals. The surface of MP-PVDF was fully covered by a thick layer of NaCl crystals, and no full-sized pillars could be identified, no obvious large NaCl crystals were found in the porous structure.

Obviously, the scaling behavior of three membranes in concentrating the NaCl solution was different, caused by the different membrane morphology and/or chemistry. A large thick layer of crystals on MP-PVDF membrane indicates that the NaCl was mainly at the membrane surface (and in the original open space between pillars), but for C-PVDF membranes, liquid might have penetrated into the support; or C-PVDF membrane was partially wetted. In MD process, external concentration polarization and temperature polarization tend to increase the possibility of NaCl nucleation at the membrane surface (Schofield et al., 1987; Martínez-Díez and Vázquez-González, 1999; Yang et al., 2015). Consequently, at a concentration factor of 1.1, the feed bulk reached salt concentration above the saturation point (Godoy et al., 2017); at the same time, the salt concentration at the membrane/liquid interface is even higher than the bulk. It is thus probable that the nucleation of NaCl occurs at membrane surface before in the bulk. Therefore, the scaling for both C-PVDF and MP-PVDF membranes is initiated from the surface rather than in from the bulk feed. Difference in the extend of scaling for C-PVDF and MP-PVDF membranes could be resulted from the different surface morphology. The micropillars in the MP-PVDF membranes surface tend to create micro turbulence (Lee et al., 2013; Jung et al., 2015; Won et al., 2016); the thick crystal layer is most probably originated from this turbulence which lead to quick nucleation of NaCl crystals, thus coverage of the membrane surface. However, C-PVDF membrane has rather homogeneous surface pores; nucleation of NaCl crystals lead to wetting, resulted in crystals in the support layer. This phenomenon has been reported and nucleation and wetting of the polypropylene membranes by NaCl concentrated solution. As a consequence, the MD flux declined as soon as the membrane was wetted (Gryta, 2002a, 2002b).

Very interesting observation was that CF_4-MP-PVDF membrane did not show any scaling or fouling, and the MD flux was very stable at a concentration factor of 1.78, far above the saturation. Assuming that the feel did not form NaCl crystals in the bulk, the solution was then super-saturated. Although supersaturation without crystallization is possible (He et al., 2009a, 2009b), one would expect that the vapor pressure of the supersaturated solution decreases; consequently, the MD flux would gradually decline. Therefore, the stable MD flux was an indication of constant feed NaCl concentration. This means that there probably was crystallization of NaCl from the feed solution after the solution was supersaturated. However, no suspension was observed in the bulk feed caused by the crystallization of NaCl in the experiment. The phenomenon will be further addressed in the next session. To unravel this puzzle is scientifically interesting and challenging, at present, we are not able to identify the origin of scalant yet. An online monitoring method will be required and the effect of the membrane surface morphology and chemistry on the scaling formation will be clarified and published in the future.

3.3. Origin of anti-scaling: hypothesis

The reduction in the contact angle is obviously caused by the scaling by NaCl. Upon saturation, C-PVDF was scaled by NaCl crystals, followed by a rapid flux decline to zero. Although the MP-PVDF membrane showed a delay to a concentration factor of 1.2, scaling was inevitable (Figs. 3 and 4 B). With such a harsh saturated solution, the clean surface of CF_4-MP-PVDF on the feed side demonstrated a surprising anti-scaling property. CF_4-MP-PVDF membranes have a very low sliding angle (Fig. 4 A-1), and their surface was repellent to water droplets. Correlation between the two phenomena raised questions: Did the water "feel" slippery at the liquid-air-polymer interface? Did this prevent the attachment of nucleation of NaCl crystals or attachment of crystals to the interface, leading to the CF_4-MP-PVDF membranes being resistant to scalant even in a supersaturated solution? In our research, however, the results of the contact angle and sliding angle have already given hints on the dynamic behavior in MD. We utilized a peristaltic pump in the experiment to give extra force to increase the release of the matters from the membrane surface for reduction of scaling. Special care was taken to prevent bulky amount of air flow into the system; but sporadically some bubbles could be visualized to enter the module. As shown in Video S1 (Supplementary information), interesting phenomena on membrane surfaces in the feed were observed: (1) for MP-PVDF membrane, bubbles were constantly seen, slowly moving along the surface in the direction of the flow; (2) for C-PVDF membrane, bubbles were seen, but mostly remaining in place; sporadically some small air bubble flowing into the module moved along the flow; (3) for CF_4-MP-PVDF membranes (the video was modified into slow motion for a clear view), there were bubbles which appeared and disappeared constantly following the pulses of the pump; moreover, a large motion of liquid-air interface was observed along the membrane surface. Above difference, though preliminary and qualitative, enlightens us on an important factor for scaling resistance for CF_4-MP-PVDF membrane.

Supplementary video related to this article can be found at https://doi.org/10.1016/j.watres.2019.01.036.

Hereby, we propose a hypothesis that the dynamics at the liquid-air-polymer interface largely dictate scaling. We first define a "stick" or "slippery" surface based on sliding angle. C-PVDF was defined as a "sticky" surface since its sliding angle is above 90° (Fig. 4 A-1). This "sticky" surface might cause non-slip of the liquid phase at the interface. For a superhydrophobic surface with a very low sliding angle, CF_4-MP-PVDF is defined as a "slippery" surface since its sliding angle is far below 10° (Fig. 4 A-1). This means that water actually "floats" above the air-polymer surface. For MP-PVDF membranes, the magnitude of stickiness or slipperiness lies between the two extremes.

Slippery surface (SLIPs) with liquid infusion has been reported for inhibition of ice nucleation or anti-ice/anti-frost performance (Kim et al. 2012, 2013; Wilson et al., 2013). The slippery surface we proposed could be identified as "an air/vapor infused surface". This logic deduction would lead to similar concept of anti-scaling for NaCl crystals. This engineered slippery liquid/air/solid interface is theoretically resistant to any crystalline particulates. We admit that the effect of the chemistry nature and nucleation/growth of the crystals to scaling for micropillared membrane is unknown and worth of further investigation. Because MD involves mass transfer, concentration and temperature polarization, it is much more complicated than the SLIPs surface created by liquid infusion (Kim et al. 2012, 2013; Wilson et al., 2013). At present, we are conducting non-intrusive observation the formation of scaling and evidence will be reported in the near future (Fortunato et al., 2018; Lee et al., 2018).

Consequently, a slippery surface is hypothesized to be scaling resistant because dynamically the liquid remains floating above the polymer phase; or the fluid solid interface is constantly changing; in other words, the liquid feels slippery at the interface. The observation of a large air/liquid interface flowing along the membrane surface was an indirect proof. However, the direct consequence is that, no crystals directly contact the polymer phase even though there are NaCl crystals in the liquid phase. Thus, the chance for scaling is low (Fig. 5). For CF_4-MP-PVDF membrane, due to the constantly moving interface, very limited interaction of the liquid and the membrane polymer could not allow the formation of nuclei on the membrane surface; even if the solution contains crystals, it is also very difficult to attach to the surface. On the contrary, for a "sticky" surface, there exists a rather static liquid-air-polymer interface; above saturation, the chance for nucleation and growth on the membrane surface increases; Driven by the concentration and temperature polarization, NaCl crystals would form on the surface and so does scaling. The in-situ observation of the dynamic scaling process at the interface remains challenging. We are currently working with other scientists using optical coherence tomography (OCT) (Fortunato et al., 2018; Lee et al., 2018) to further confirm the observation and compare different surface morphology on the scaling for various inorganic salts.

The other quantitative measure of the slipperiness of hydrophobic soft polymeric membrane surfaces has not yet been established in the literature. Nevertheless, the measurement of slipperiness of superhydrophobic surface has been reported as the slip length based on Navier's model (Granick et al., 2003; Choi et al., 2006). Measurement of the slip length of a surface would indirectly support the present correlation of slip and scaling. Beyond scaling, the investigation of current slippery surface is useful for quantifying the flow resistance of the inner surface of a channel (Choi et al., 2006; Truesdell et al., 2006; Daniello et al., 2009; Haase et al., 2016). Low friction has been shown at a nanopatterned surface (Cottin-Bizonne et al., 2003), which might be related to the formation of "nanobubbles" that gave rise to reduced friction resulting in a slippery surface (Tyrrell and Attard, 2001; Shin et al., 2015). As shown in video S1 (Supplementary information), we didn't observe nanobubbles, but a moving air/liquid interface along the superhydrophobic CF_4-MP-PVDF membrane surface. This observation provided a qualitative proof of the possible slippery character at the interface. Yet, the scientific evidence requires further experimental verification of the slip length and simulation of the flow pattern. The fundamental dynamic mechanism of scaling in membrane distillation could then be clarified. Understanding the dynamic scaling resistance might also shed light on fouling by other organic matter. This assumption lies in the probability of interaction between the foulant (in the feed) and the membrane materials. If direct contact between the membrane materials and the feed fouling is largely suppressed, fouling resistance might be observed.

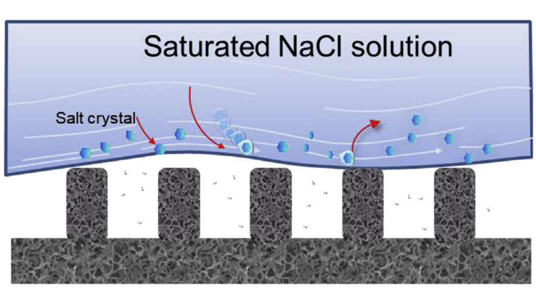

Fig. 5. Schematic of the slippery interface in relation to anti-scaling for CF_4-MP-PVDF membrane.

4. Conclusion remarks

Superhydrophobic polyvinylidene fluoride (PVDF) membranes with micropillar arrays (MP-PVDF) were created via a micromolding phase separation (μPS) technology, providing a simple method for creating well-controlled surface morphology. With an additional CF_4 plasma treatment of MP-PVDF, the resultant CF_4-MP-PVDF had a significantly increased contact angle (174°) and decreased sliding angle (3.0°). This CF_4-MP-PVDF membrane showed less scaling upon concentrating highly saline NaCl solution (25 wt%) by direct contact membrane distillation. In contrast, both commercial PVDF and MP-PVDF membranes showed severe scaling followed by flux reduction. Membrane autopsy showed that scaling by NaCl crystals and possible wetting occurred in C-PVDF and MP-PVDF, but not CF_4-MP-PVDF membranes. Visual observation of a floating water/air interface in CF_4-MP-PVDF membranes qualitatively demonstrated that a slippery surface might contribute to resistance to scaling. We hypothetically correlate the sliding angle to the slippery surface of CF_4-MP-PVDF and its anti-scaling properties. This work may provide a platform and methodology for understanding scaling beyond membrane distillation.

Acknowledgements

The research is supported by Newton Advanced Fellowship (Grant No. NA170113) and National Natural Science Foundation of China (No. U1507117, 21676290, 51861145313). Zechun Xiao and Rui Zheng contributed equally to the experimental work.

Appendix A. Supplementary data

Supplementary data to this article can be found online at https://doi.org/10.1016/j.watres.2019.01.036.

References

Alkhudhiri, A., Darwish, N., Hilal, N., 2012. Membrane distillation: a comprehensive review. Desalination 287, 2–18.
Boo, C., Lee, J., Elimelech, M., 2016a. Engineering surface energy and nanostructure of microporous films for expanded membrane distillation applications. Environ. Sci. Technol. 50 (15), 8112–8119.
Boo, C., Lee, J., Elimelech, M., 2016b. Omniphobic polyvinylidene fluoride (PVDF) membrane for desalination of shale gas produced water by membrane distillation. Environ. Sci. Technol. 50 (22), 12275–12282.
Bouchrit, R., Boubakri, A., Hafiane, A., Bouguecha, S.A.-T., 2015. Direct contact membrane distillation: capability to treat hyper-saline solution. Desalination 376, 117–129.
Bouchrit, R., Boubakri, A., Mosbahi, T., Hafiane, A., Bouguecha, S.A.-T., 2017. Membrane crystallization for mineral recovery from saline solution: study case Na2SO4 crystals. Desalination 412, 1–12.
Chen, G., Lu, Y., Yang, X., Wang, R., Fane, A.G., 2014. Quantitative study on crystallization-induced scaling in high-concentration direct-contact membrane distillation. Ind. Eng. Chem. Res. 53 (40), 15656–15666.
Chen, G., Wang, Z., Nghiem, L.D., Li, X.-M., Xie, M., Zhao, B., Zhang, M., Song, J., He, T., 2015. Treatment of shale gas drilling flowback fluids (SGDFs) by forward osmosis: membrane fouling and mitigation. Desalination 366, 113–120.
Chen, Y., Tian, M., Li, X., Wang, Y., An, A.K., Fang, J., He, T., 2017a. Anti-wetting behavior of negatively charged superhydrophobic PVDF membranes in direct contact membrane distillation of emulsified wastewaters. J. Membr. Sci. 535, 230–238.
Chen, Y., Zheng, R., Wang, J., Liu, Y., Wang, Y., Li, X.-M., He, T., 2017b. Laminated PTFE membranes to enhance the performance in direct contact membrane distillation for high salinity solution. Desalination 424, 140–148.
Choi, C.-H., Ulmanella, U., Kim, J., Ho, C.-M., Kim, C.-J., 2006. Effective slip and friction reduction in nanograted superhydrophobic microchannels. Phys. Fluids 18 (8), 087105.
Choi, J., Choi, Y., Jang, Y., Shin, Y., Lee, S., 2017. Effect of aeration on CaSO4 scaling in membrane distillation process. Desalination Water Treat. 90, 7–15.
Choi, Y., Naidu, G., Jeong, S., Lee, S., Vigneswaran, S., 2018. Effect of chemical and physical factors on the crystallization of calcium sulfate in seawater reverse osmosis brine. Desalination 426, 78–87.
Cottin-Bizonne, C., Barrat, J.L., Bocquet, L., Charlaix, E., 2003. Low-friction flows of liquid at nanopatterned interfaces. Nat. Mater. 2 (4), 237–240.
Çulfaz, P.Z., Rolevink, E., van Rijn, C., Lammertink, R.G.H., Wessling, M., 2010.

Microstructured hollow fibers for ultrafiltration. J. Membr. Sci. 347 (1–2), 32–41.
Çulfaz, P.Z., Haddad, M., Wessling, M., Lammertink, R.G.H., 2011a. Fouling behavior of microstructured hollow fibers in cross-flow filtrations: critical flux determination and direct visual observation of particle deposition. J. Membr. Sci. 372 (1–2), 210–218.
Çulfaz, P.Z., Wessling, M., Lammertink, R.G.H., 2011b. Hollow fiber ultrafiltration membranes with microstructured inner skin. J. Membr. Sci. 369 (1–2), 221–227.
Daniello, R.J., Waterhouse, N.E., Rothstein, J.P., 2009. Drag reduction in turbulent flows over superhydrophobic surfaces. Phys. Fluids 21 (8), 085103.
Deshmukh, A., Boo, C., Karanikola, V., Lin, S., Straub, A.P., Tong, T., Warsinger, D.M., Elimelech, M., 2018. Membrane distillation at the water-energy nexus: limits, opportunities, and challenges. Energy Environ. Sci. 11, 1177–1196.
Duong, H.C., Hai, F.I., Al-Jubainawi, A., Ma, Z., He, T., Nghiem, L.D., 2017. Liquid desiccant lithium chloride regeneration by membrane distillation for air conditioning. Separ. Purif. Technol. 177, 121–128.
Edwie, F., Chung, T.-S., 2013. Development of simultaneous membrane distillation-crystallization (SMDC) technology for treatment of saturated brine. Chem. Eng. Sci. 98, 160–172.
ElSherbiny, I.M.A., Khalil, A.S.G., Ulbricht, M., 2017. Surface micro-patterning as a promising platform towards novel polyamide thin-film composite membranes of superior performance. J. Membr. Sci. 529, 11–22.
Eykens, L., De Sitter, K., Dotremont, C., Pinoy, L., Van der Bruggen, B., 2017. Membrane synthesis for membrane distillation: a review. Separ. Purif. Technol. 182, 36–51.
Eykens, L., Hitsov, I., De Sitter, K., Dotremont, C., Pinoy, L., Nopens, I., Van der Bruggen, B., 2016. Influence of membrane thickness and process conditions on direct contact membrane distillation at different salinities. J. Membr. Sci. 498, 353–364.
Fortunato, L., Jang, Y., Lee, J.-G., Jeong, S., Lee, S., Leiknes, T., Ghaffour, N., 2018. Fouling development in direct contact membrane distillation: non-invasive monitoring and destructive analysis. Water Res. 132, 34–41.
Gençal, Y., Durmaz, E.N., Çulfaz-Emecen, P.Z., 2015. Preparation of patterned microfiltration membranes and their performance in crossflow yeast filtration. J. Membr. Sci. 476, 224–233.
Godoy, A.A., Carvalho, L. B. d., Kummrow, F., Pamplin, P.A.Z., 2017. Sodium chloride as a reference substance for the three growth endpoints used in the Lemna minor L.(1753) test. Revista Ambiente & Água 12 (1), 8–16.
Granick, S., Zhu, Y., Lee, H., 2003. Slippery questions about complex fluids flowing past solids. Nat. Mater. 2, 221–227.
Gryta, M., 2002a. Concentration of NaCl solution by membrane distillation integrated with crystallization. Separ. Sci. Technol. 37 (15), 3535–3558.
Gryta, M., 2002b. Direct contact membrane distillation with crystallization applied to NaCl solutions. Chem. Pap.-Slovak Acad. Sci. 56 (1), 14–19.
Gryta, M., 2008. Fouling in direct contact membrane distillation process. J. Membr. Sci. 325 (1), 383–394.
Gryta, M., 2010. Desalination of thermally softened water by membrane distillation process. Desalination 257 (1), 30–35.
Gryta, M., 2011. The influence of magnetic water treatment on CaCO3 scale formation in membrane distillation process. Separ. Purif. Technol. 80 (2), 293–299.
Gryta, M., 2016. Degradation of polypropylene membranes applied in membrane distillation crystallizer. Crystals 6 (4).
Haase, A.S., Wood, J.A., Lammertink, R.G.H., Snoeijer, J.H., 2016. Why bumpy is better: the role of the dissipation distribution in slip flow over a bubble mattress. Phys. Rev. Fluid. 1 (5).
Hashino, M., Katagiri, T., Kubota, N., Ohmukai, Y., Maruyama, T., Matsuyama, H., 2011. Effect of surface roughness of hollow fiber membranes with gear-shaped structure on membrane fouling by sodium alginate. J. Membr. Sci. 366 (1–2), 389–397.
He, F., Gilron, J., Sirkar, K.K., 2013. High water recovery in direct contact membrane distillation using a series of cascades. Desalination 323, 48–54.
He, F., Sirkar, K.K., Gilron, J., 2009a. Effects of antiscalants to mitigate membrane scaling by direct contact membrane distillation. J. Membr. Sci. 345 (1), 53–58.
He, F., Sirkar, K.K., Gilron, J., 2009b. Studies on scaling of membranes in desalination by direct contact membrane distillation: CaCO3 and mixed CaCO3/CaSO4 systems. Chem. Eng. Sci. 64 (8), 1844–1859.
He, T., Mulder, M.H.V., Wessling, M., 2003. Preparation of porous hollow fiber membranes with a triple-orifice spinneret. J. Appl. Polym. Sci. 87 (13), 2151–2157.
Hickenbottom, K.L., Cath, T.Y., 2014. Sustainable operation of membrane distillation for enhancement of mineral recovery from hypersaline solutions. J. Membr. Sci. 454, 426–435.
Jamshidi Gohari, R., Lau, W.J., Matsuura, T., Ismail, A.F., 2013. Effect of surface pattern formation on membrane fouling and its control in phase inversion process. J. Membr. Sci. 446, 326–331.
Jentzsch, P.V., Ciobotă, V., Kampe, B., Rösch, P., Popp, J., 2011. Origin of salt mixtures and mixed salts in atmospheric particulate matter. J. Raman Spectrosc. 43 (4), 514–519.
Ji, X., Curcio, E., Al Obaidani, S., Di Profio, G., Fontananova, E., Drioli, E., 2010a. Membrane distillation-crystallization of seawater reverse osmosis brines. Separ. Purif. Technol. 71 (1), 76–82.
Ji, Y., Li, X.-M., Yin, Y., Zhang, Y.-Y., Wang, Z.-W., He, T., 2010b. Morphological control and cross-flow filtration of microfiltration membranes prepared via a sacrificial-layer approach. J. Membr. Sci. 353 (1–2), 159–168.
Jiang, X., Tuo, L., Lu, D., Hou, B., Chen, W., He, G., 2017. Progress in membrane distillation crystallization: process models, crystallization control and innovative applications. Front. Chem. Sci. Eng. 11 (4), 647–662.
Julian, H., Ye, Y., Li, H., Chen, V., 2018. Scaling mitigation in submerged vacuum membrane distillation and crystallization (VMDC) with periodic air-backwash. J. Membr. Sci. 547, 19–33.
Jung, S.Y., Won, Y.-J., Jang, J.H., Yoo, J.H., Ahn, K.H., Lee, C.-H., 2015. Particle deposition on the patterned membrane surface: simulation and experiments. Desalination 370, 17–24.
Junghyun, K., Heejung, K., Seockheon, L., Sangho, L., Seungkwan, H., 2017. Membrane distillation (MD) integrated with crystallization (MDC) for shale gas produced water (SGPW) treatmentjournal. Desalination 403, 172–178.
Kharraz, J.A., Bilad, M.R., Arafat, H.A., 2015. Flux stabilization in membrane distillation desalination of seawater and brine using corrugated PVDF membranes. J. Membr. Sci. 495, 404–414.
Kim, J., Kim, J., Hong, S., 2018. Recovery of water and minerals from shale gas produced water by membrane distillation crystallization. Water Res. 129, 447–459.
Kim, J.U., Lee, S., Kim, T.-i., 2016. Recent advances in unconventional lithography for challenging 3D hierarchical structures and their applications. J. Nanomater. 1–17, 7602395. http://dx.doi.org/10.1155/2016/7602395.
Kim, P., Kreder, M.J., Alvarenga, J., Aizenberg, J., 2013. Hierarchical or not? Effect of the length scale and hierarchy of the surface roughness on omniphobicity of lubricant-infused substrates. Nano Lett. 13 (4), 1793–1799.
Kim, P., Wong, T.-S., Alvarenga, J., Kreder, M.J., Adorno-Martinez, W.E., Aizenberg, J., 2012. Liquid-infused nanostructured surfaces with extreme anti-ice and anti-frost performance. ACS Nano 6 (8), 6569–6577.
Latorre, M., 2005. Environmental impact of brine disposal on Posidonia seagrasses. Desalination 182 (1), 517–524.
Lee, C., Choi, C.H., Kim, C.-J., 2016c. Superhydrophobic drag reduction in laminar flows: a critical review. Exp. Fluid 57–176.
Lee, E.-J., An, A.K., He, T., Woo, Y.C., Shon, H.K., 2016a. Electrospun nanofiber membranes incorporating fluorosilane-coated TiO2 nanocomposite for direct contact membrane distillation. J. Membr. Sci. 520, 145–154.
Lee, J.-G., Jang, Y., Fortunato, L., Jeong, S., Lee, S., Leiknes, T., Ghaffour, N., 2018. An advanced online monitoring approach to study the scaling behavior in direct contact membrane distillation. J. Membr. Sci. 546, 50–60.
Lee, J., Boo, C., Ryu, W.H., Taylor, A.D., Elimelech, M., 2016b. Development of omniphobic desalination membranes using a charged electrospun nanofiber scaffold. ACS Appl. Mater. Interfaces 8 (17), 11154–11161.
Li, H., Wang, H., Liu, Q., Tan, Y., Jiang, N., Lin, Y., 2016. Evaporation process for treating high-salinity industrial wastewater at low temperatures and ambient pressure. Desalination Water Treat. 57 (56), 27048–27060.
Lee, Y.K., Won, Y.-J., Yoo, J.H., Ahn, K.H., Lee, C.-H., 2013. Flow analysis and fouling on the patterned membrane surface. J. Membr. Sci. 427, 320–325.
Li, X.-M., He, T., Crego-Calama, M., Reinhoudt, D.N., 2008a. Conversion of a metastable superhydrophobic surface to an ultraphobic surface. Langmuir 24 (15), 8008–8012.
Li, X.M., Ji, Y., He, T., Wessling, M., 2008b. A sacrificial-layer approach to prepare microfiltration membranes. J. Membr. Sci. 320 (1–2), 1–7.
Li, X.-M., Ji, Y., Yin, Y., Zhang, Y.-Y., Wang, Y., He, T., 2010. Origin of delamination/adhesion in polyetherimide/polysulfone co-cast membranes. J. Membr. Sci. 352 (1–2), 173–179.
Li, X.-M., Reinhoudt, D., Crego-Calama, M., 2007. What do we need for a superhydrophobic surface? A review on the recent progress in the preparation of superhydrophobic surfaces. Chem. Soc. Rev. 36 (8), 1350–1368.
Lin, S., Nejati, S., Boo, C., Hu, Y., Osuji, C.O., Elimelech, M., 2014. Omniphobic membrane for robust membrane distillation. Environ. Sci. Technol. Lett. 1 (11), 443–447.
Martínez-Díez, L., Vázquez-González, M.I., 1999. Temperature and concentration polarization in membrane distillation of aqueous salt solutions. J. Membr. Sci. 156 (2), 265–273.
Maruf, S.H., Greenberg, A.R., Ding, Y., 2016. Influence of substrate processing and interfacial polymerization conditions on the surface topography and permselective properties of surface-patterned thin-film composite membranes. J. Membr. Sci. 512, 50–60.
Meng, S., Mansouri, J., Ye, Y., Chen, V., 2014a. Effect of templating agents on the properties and membrane distillation performance of TiO2-coated PVDF membranes. J. Membr. Sci. 450, 48–59.
Meng, S., Ye, Y., Mansouri, J., Chen, V., 2014b. Fouling and crystallisation behaviour of superhydrophobic nano-composite PVDF membranes in direct contact membrane distillation. J. Membr. Sci. 463, 102–112.
Meng, S., Ye, Y., Mansouri, J., Chen, V., 2015. Crystallization behavior of salts during membrane distillation with hydrophobic and superhydrophobic capillary membranes. J. Membr. Sci. 473, 165–176.
Naidu, G., Jeong, S., Vigneswaran, S., 2014. Influence of feed/permeate velocity on scaling development in a direct contact membrane distillation. Separ. Purif. Technol. 125, 291–300.
Naidu, G., Zhong, X., Vigneswaran, S., 2018. Comparison of membrane distillation and freeze crystallizer as alternatives for reverse osmosis concentrate treatment. Desalination 427, 10–18.
Nariyoshi, Y.N., Pantoja, C.E., Seckler, M.M., 2016. Evaluation of sodium chloride crystallization in membrane distillation crystallization applied to water desalination. Braz. J. Chem. Eng. 33 (3), 675–690.
Nejati, S., Boo, C., Osuji, C.O., Elimelech, M., 2015. Engineering flat sheet

microporous PVDF films for membrane distillation. J. Membr. Sci. 492, 355–363.
Nghiem, L.D., Hildinger, F., Hai, F.I., Cath, T., 2011. Treatment of saline aqueous solutions using direct contact membrane distillation. Desalination Water Treat. 32 (1–3), 234–241.
Ramezanianpour, M., Sivakumar, M., 2014. An analytical flux decline model for membrane distillation. Desalination 345, 1–12.
Razmjou, A., Arifin, E., Dong, G., Mansouri, J., Chen, V., 2012. Superhydrophobic modification of TiO2 nanocomposite PVDF membranes for applications in membrane distillation. J. Membr. Sci. 415, 850–863.
Ren, L.-F., Xia, F., Chen, V., Shao, J., Chen, R., He, Y., 2017. TiO2-FTCS modified superhydrophobic PVDF electrospun nanofibrous membrane for desalination by direct contact membrane distillation. Desalination 423, 1–11.
Schofield, R.W., Fane, A.G., Fell, C.J.D., 1987. Heat and mass transfer in membrane distillation. J. Membr. Sci. 33 (3), 299–313.
Shannon, M.A., Bohn, P.W., Elimelech, M., Georgiadis, J.G., Mariñas, B.J., Mayes, A.M., 2008. Science and technology for water purification in the coming decades. Nature 452, 301–310.
Shin, D.H., Park, J.B., Kim, Y.J., Kim, S.J., Kang, J.H., Lee, B., Cho, S.P., Hong, B.H., Novoselov, K.S., 2015. Growth dynamics and gas transport mechanism of nanobubbles in graphene liquid cells. Nat. Commun. 6.
Shin, Y., Sohn, J., 2016. Mechanisms for scale formation in simultaneous membrane distillation crystallization: effect of flow rate. J. Ind. Eng. Chem. 35, 318–324.
Tang, L., Iddya, A., Zhu, X., Dudchenko, A.V., Duan, W., Turchi, C., Vanneste, J., Cath, T.Y., Jassby, D., 2017. Enhanced flux and electrochemical cleaning of silicate scaling on carbon nanotube-coated membrane distillation membranes treating geothermal brines. ACS Appl. Mater. Interfaces 9 (44), 38594–38605.
Tian, M., Li, X., Yin, Y., He, T., Liu, J., 2015a. Preparaton of superhydrophobic membranes and their application in membrane distillation. Prog. Chem. 27 (8), 1033–1041.
Tian, M., Yin, Y., Yang, C., Zhao, B., Song, J., Liu, J., Li, X.-M., He, T., 2015b. CF4 plasma modified highly interconnective porous polysulfone membranes for direct contact membrane distillation (DCMD). Desalination 369, 105–114.
Tijing, L.D., Woo, Y.C., Choi, J.-S., Lee, S., Kim, S.-H., Shon, H.K., 2015. Fouling and its control in membrane distillation-A review. J. Membr. Sci. 475, 215–244.
Tijing, L.D., Woo, Y.C., Shim, W.-G., He, T., Choi, J.-S., Kim, S.-H., Shon, H.K., 2016. Superhydrophobic nanofiber membrane containing carbon nanotubes for high-performance direct contact membrane distillation. J. Membr. Sci. 502, 158–170.
Truesdell, R., Mammoli, A., Vorobieff, P., van Swol, F., Brinker, C.J., 2006. Drag reduction on a patterned superhydrophobic surface. Phys. Rev. Lett. 97 (4), 044504.
Tun, C.M., Fane, A.G., Matheickal, J.T., Sheikholeslami, R., 2005. Membrane distillation crystallization of concentrated salts—flux and crystal formation. J. Membr. Sci. 257 (1), 144–155.
Tyree, C.A., Hellion, V.M., Alexandrova, O.A., Allen, J.O., 2007. Foam droplets generated from natural and artificial seawaters. J. Geophys. Res.: Atmospheres 112 (D12).
Tyrrell, J.W.G., Attard, P., 2001. Images of nanobubbles on hydrophobic surfaces and their interactions. Phys. Rev. Lett. 87 (17), 176104.
Wang, Z.X., Hou, D.Y., Lin, S.H., 2016a. Composite membrane with underwater-oleophobic surface for anti-oil-fouling membrane distillation. Environ. Sci. Technol. 50 (7), 3866–3874.
Wang, Z.X., Jin, J., Hou, D.Y., Lin, S.H., 2016b. Tailoring surface charge and wetting property for robust oil-fouling mitigation in membrane distillation. J. Membr. Sci. 516, 113–122.
Warsinger, D.M., Servi, A., Van Belleghem, S., Gonzalez, J., Swaminathan, J., Kharraz, J., Chung, H.W., Arafat, H.A., Gleason, K.K., Lienhard, J.H.V., 2016. Combining air recharging and membrane superhydrophobicity for fouling prevention in membrane distillation. J. Membr. Sci. 505, 241–252.
Wei, X., Zhao, B., Li, X.-M., Wang, Z., He, B.-Q., He, T., Jiang, B., 2012. CF4 plasma surface modification of asymmetric hydrophilic polyethersulfone membranes for direct contact membrane distillation. J. Membr. Sci. 407–408, 164–175.
Wilson, P.W., Lu, W., Xu, H., Kim, P., Kreder, M.J., Alvarenga, J., Aizenberg, J., 2013. Inhibition of ice nucleation by slippery liquid-infused porous surfaces (SLIPS). Phys. Chem. Chem. Phys. 15 (2), 581–585.
Won, Y.-J., Jung, S.-Y., Jang, J.-H., Lee, J.-W., Chae, H.-R., Choi, D.-C., Hyun Ahn, K., Lee, C.-H., Park, P.-K., 2016. Correlation of membrane fouling with topography of patterned membranes for water treatment. J. Membr. Sci. 498, 14–19.
Won, Y.J., Lee, J., Choi, D.C., Chae, H.R., Kim, I., Lee, C.H., Kim, I.C., 2012. Preparation and application of patterned membranes for wastewater treatment. Environ. Sci. Technol. 46 (20), 11021–11027.
Xie, M., Luo, W., Gray, S.R., 2017. Surface pattern by nanoimprint for membrane fouling mitigation: design, performance and mechanisms. Water Res. 124, 238–243.
Xing, L., Song, J., Li, Z., Liu, J., Huang, T., Dou, P., Chen, Y., Li, X.-M., He, T., 2016. Solvent stable nanoporous poly (ethylene-co-vinyl alcohol) barrier membranes for liquid-liquid extraction of lithium from a salt lake brine. J. Membr. Sci. 520, 596–606.
Xue Mei Li, M.C.C., 2007. The rough with the smooth. Chem. Sci. 4, C75.
Yang, C., Li, X.-M., Gilron, J., Kong, D.-f., Yin, Y., Oren, Y., Linder, C., He, T., 2014. CF4 plasma-modified superhydrophobic PVDF membranes for direct contact membrane distillation. J. Membr. Sci. 456, 155–161.
Yang, C., Tian, M., Xie, Y., Li, X.-M., Zhao, B., He, T., Liu, J., 2015. Effective evaporation of CF4 plasma modified PVDF membranes in direct contact membrane distillation. J. Membr. Sci. 482, 25–32.
Yun, Y., Ma, R., Zhang, W., Fane, A.G., Li, J., 2006. Direct contact membrane distillation mechanism for high concentration NaCl solutions. Desalination 188 (1), 251–262.
Zou, T., Dong, X., Kang, G., Zhou, M., Li, M., Cao, Y., 2018. Fouling behavior and scaling mitigation strategy of CaSO4 in submerged vacuum membrane distillation. Desalination 425, 86–93.